

# Potential Power of the Pyramidal Structure IV: Discovery of Entanglement Due to Pyramid Effects

Osamu Takagi<sup>1</sup>, Masamichi Sakamoto<sup>2</sup>, Kimiko Kawano<sup>1</sup>, Mikio Yamamoto<sup>1</sup>

<sup>1</sup>International Research Institute (IRI), Chiba, Japan; <sup>2</sup>Aquavision Academy, Chiba, Japan

**Correspondence to:** Osamu Takagi, takagi@a-iri.org

**Keywords:** Pyramid, Potential Power, Entanglement, Meditation, Non-Contact Effect, Biosensor, *Cucumis sativus*, Gas, Psi Index

**Received:** June 10, 2021

**Accepted:** July 24, 2021

**Published:** July 27, 2021

Copyright © 2021 by author(s) and Scientific Research Publishing Inc.

This work is licensed under the Creative Commons Attribution International License (CC BY 4.0).

<http://creativecommons.org/licenses/by/4.0/>



Open Access

## ABSTRACT

Since October 2007, we have been conducting rigorous scientific research on the unexplained “power” of a pyramidal structure (PS). From our research results so far, we could classify pyramid effects by the PS into the following two types: (i) the pyramid effects due to the potential power of the PS and (ii) the pyramid effects due to the influence of the test subject meditating inside the PS. We have been using edible cucumber sections as the biosensors. The pyramid effect existence was clarified by measuring and analyzing the concentration of volatile components released from the biosensors. The biosensors were arranged as a pair: one member of the pair was placed at the PS apex and the other was placed at the calibration control point 8.0 m away from the PS. In this paper, we report a new discovery regarding the type (i) pyramid effects. We discovered a phenomenon considered to be entanglement between the biosensor pairs detecting the pyramid effects. In other words, the biosensors at the PS apex, which were affected by the potential power of the PS, affected the biosensors at the calibration control point. We also confirmed that the effects on the biosensors placed at the calibration control point were not due to the potential power of the PS. Furthermore, we showed that the magnitude of the effect of entanglement changed with the seasons. We expect that our research results will be widely accepted in the future and will become the foundation for a new research field in science, with a wide range of applications.

## 1. INTRODUCTION

Since October 2007, we have been conducting rigorous scientific research on the unexplained “power” of a pyramidal structure (PS). From research results of our nine original papers published so far, we could classify the pyramid effects by the PS into the following two types [1-9]: (i) the pyramid effects due to the potential power of the PS and (ii) the pyramid effects due to the influence of the test subject medi-

tating inside the PS. Regarding the type (i) pyramid effects, the following three results have been obtained so far. 1) We clarified the existence of the pyramid effects on the biosensors placed at the PS apex due to the potential power of the PS. The annual data ( $n = 468$ ) were divided into two periods by the spring equinox and the autumn equinox, and the pyramid effects of each were compared. As a result,  $p = 6.0 \times 10^{-3}$ , was obtained, which was a statistically significant difference (Welch's t-test, two-tails; the same test was used to obtain the p-values given hereafter) [7]. 2) We clarified that the potential power of the PS affected the biosensors placed in two layers at the PS apex, and the pyramid effects differed between the lower and the upper layers. The psi index  $\Psi$ , which indicates the magnitude of the pyramid effects, had a negative value of  $-3.01$  for the lower biosensors, and a positive value of  $5.52$  for the upper biosensors. There was a significant difference between the lower and upper pyramid effects,  $p = 4.0 \times 10^{-7}$  [8]. 3) As a result of analyzing the annual data by dividing it into four seasons of winter, spring, summer and autumn, we clarified that there were two types of pyramid effects with and without seasonal variation. As a result of comparing winter and summer with respect to the pyramid effects that changed with the seasons,  $p = 1.8 \times 10^{-3}$  was obtained, which was a statistically significant difference [9].

In this paper, we report a new discovery regarding type (i) pyramid effects. We have expressed the magnitude of the pyramid effects by an index called the psi index calculated from the volatile components (gas concentration) released from the biosensors. With the introduction of the psi index, it has become possible to quantitatively assess the "healing power" [10-12] and "pyramid power" [1-3, 6-9] of unexplained phenomena, and to perform scientific analyses. However, in this paper, we did not introduce the psi index, but rather analyzed the gas concentration. As a result, we discovered a phenomenon considered to be entanglement between pairs of the biosensors, which was overlooked when the psi index was used. The biosensors at the PS apex, that is, the experimental samples, were affected by the potential power of the PS. And by this entanglement, the biosensors at the PS apex affected the biosensors, that is, the control samples at the calibration control point. We also confirmed that the effects on the biosensors placed at the calibration control point were not due to the potential power of the PS. Furthermore, we showed that the magnitude of the effect of entanglement changed with the seasons.

The psi index has been considered as an index showing the magnitude of the pyramid effects on experimental samples placed at the PS apex. But this time, the discovery of entanglement between the biosensors has added new knowledge to the psi index. That is, the psi index includes not only the pyramid effects on the experimental samples placed at the PS apex, but also the influence on the control samples by entanglement.

Our purpose is to verify the existence of the potential power of the PS alone by experiment when excluding the effects of the test subject. In the future, we expect that these results will be widely recognized, and they will become the basis for a new research field in science, with a wide range of applications.

## 2. EXPERIMENT

We used biosensors made by cutting the cucumber fruit, *Cucumis sativus*, to verify the pyramid effect. The biosensors were placed at the PS apex and calibration control point for 30 minutes. Then, the volatile components (gas concentration) released from the biosensors affected at each location were measured. The reason why cucumber sections can be used as biosensors for detecting the pyramid effects is described as follows. In general, it is known that plants exhibit a biological defense/repair reaction when they are injured for some reason, such as being eaten by insects [13-16]. It has been reported that when vegetables and fruits have been harvested for food, and even after a week or more, if they are damaged by cutting, etc., they show a biological defense/repair reaction for a certain period of time [17]. By this biological defense/repair reaction, volatile components are released from the cut surface of the cucumber fruit, and biophotons are generated. This biological reaction is a very complicated and delicate chemical reaction, and it is considered that it reacts sensitively to subtle changes in the external environment that are difficult to measure with a physical measuring instrument. Therefore, we speculated that the cucumber section could be used as an environment-responsive high-sensitivity biosensor. In the experiment, the cucumbers

were cut to create biosensors, which were placed at the PS apex and calibration control point about 10 minutes later. They were kept at the apex and control point for 30 minutes. Therefore, while the biological reaction on the cut surface continues, the biosensors are affected by the environment of the PS apex and the calibration control point. We consider that the gas concentration proportional to the environmental state of the PS apex and the calibration control point is detected.

We have introduced the psi index as an indicator of the magnitude of the pyramid effects. The psi index is calculated by the natural logarithm of the ratio of the gas concentrations of pair samples, experimental samples and control samples, having the same cut surface (Equation (2), given in Section 4). The paired samples are very similar samples, except that the orientation of the cut surface is different. Therefore, the psi index quantitatively reveals the difference between the environment in which the experimental samples and the control samples are placed. However, the individual cucumbers used in each experiment are different, and it is expected that the external environment conditions such as temperature, humidity, and geomagnetism of the laboratory will be different for each experiment. Therefore, the biosensors at the calibration control point were regarded as a reference, and the psi index was calibrated. By calibrating the psi index, it was possible to offset the differences in environmental changes between experiments. This made it possible for the calibrated psi index to detect only the difference in the environment in which the experimental samples and the control samples were placed. If the calibrated psi index is positive, it can be determined that the environment in which the experimental samples are placed is the environment in which gas production is promoted more as compared with the environment in which the control samples are placed. On the contrary, if the calibrated psi index is negative, it can be determined that the environment in which the experimental samples are placed is the environment in which gas production is suppressed as compared with the environment in which the control samples are placed. In this way, the calibrated psi index is an excellent index that can quantitatively capture the difference in the environment in which the biosensors are placed, and it has been used to detect the pyramid effects. However, in this paper, we tried to detect the pyramid effects only by analyzing the gas concentration without using the psi index. As a result, we discovered the phenomenon of entanglement between paired samples, which could not have been seen when using the psi index.

## 2.1. Biosensors

**Figure 1(a)** and **Figure 1(b)** show how to make the biosensors from commercially available edible cucumbers for one trial experiment. Four cucumbers were used for one trial experiment. In **Figure 1(a)**, after cutting off 3 - 5 cm on the vine side of the first cucumber A, four 2 cm wide sections were prepared. The 2 cm section A1 closest to the vine side was cut in half and placed on Petri dishes  $G_{E1}$  and  $G_{C1}$  so that the cut surfaces were on the upper surface. Here,  $G_{E1}$  and  $G_{C1}$  were considered as a pair. The second 2 cm section A2 from the vine side was also cut in half and placed on Petri dishes  $G_{E2}$  and  $G_{C2}$ . Similarly, the third and fourth 2 cm sections A3 and A4 from the vine side were also placed on Petri dishes  $G_{E3}$ ,  $G_{C3}$  and  $G_{E4}$ ,  $G_{C4}$ . The second cucumber B to the fourth cucumber D were cut in the same manner, and the sections were placed on Petri dishes. However, each time the individual cucumber being cut was changed, the order of the sections placed on the Petri dish was changed, section B1 was placed on  $G_{E2}$  and  $G_{C2}$ , section C1 was placed on  $G_{E3}$  and  $G_{C3}$ , etc. Finally, the Pair1-Pair4 biosensors were created in which eight Petri dishes contained four cucumber sections each. Here, the pair number was arbitrary, and after placing 4 cucumber sections in 8 Petri dishes, the die was rolled to determine pairs 1 to 4. In the case of pairs, the upper surface of the  $G_E$  and  $G_C$  cucumber sections placed on the Petri dishes was the same cut surface, but the direction of the axes was different. The direction of the upper surface of the cucumber section placed on the Petri dish was defined as the direction from the lower surface in contact with the Petri dish to the upper surface. At this time, the upper surface of the section placed on the  $G_E$  was in the same direction as the growth axis of the cucumber. In addition, the upper surface of the section placed on the  $G_C$  was in the direction opposite to the growth axis. The growth axis of the cucumber was the direction from the vine side to the flower side of the cucumber fruit. From the experimental results so far, we clarified that the gas concentration

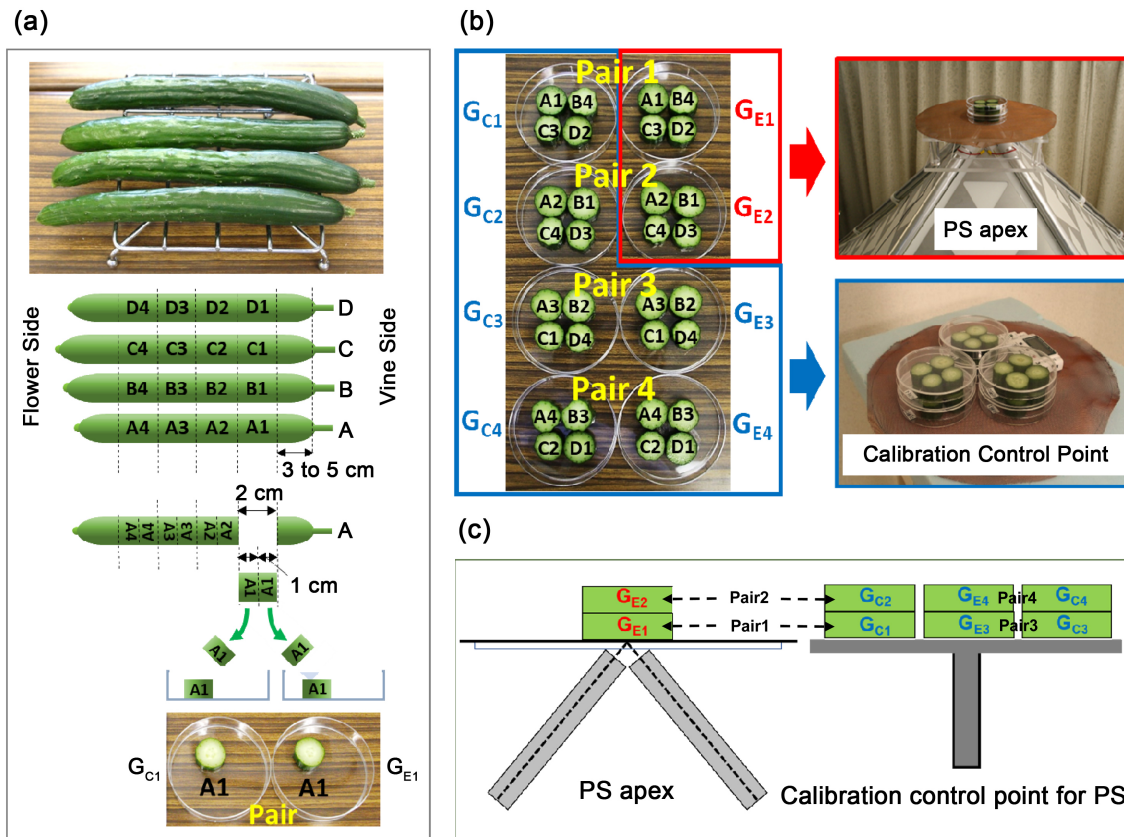


**Figure 1.** How to prepare and place the biosensors for the experiment.

differed depending on the direction of the cut surface, and  $G_E < G_C$  [5]. In addition,  $G_E$  were experimental samples, and  $G_C$  were control samples. Arbitrarily determined Pair1 and Pair2 experimental samples  $G_{E1}$  and  $G_{E2}$  were placed at the PS apex in two layers. Pair1 and Pair2 control samples  $G_{C1}$ ,  $G_{C2}$  and Pair3 and Pair4 experimental and control samples  $G_{E3}$ ,  $G_{E4}$ ,  $G_{C3}$ ,  $G_{C4}$  were placed in two layers at a calibration control point 8.0 m away from the PS (Figure 1(b)). Therefore, the experimental samples  $G_{E1}$ ,  $G_{E2}$  and the control samples  $G_{C1}$ ,  $G_{C2}$  in Pair1 and Pair2 were placed 8.0 m apart. On the other hand, the experimental samples  $G_{E3}$ ,  $G_{E4}$  and the control samples  $G_{C3}$ ,  $G_{C4}$  of Pair3 and Pair4 were both placed at the calibration control point, and the Petri dishes are in contact with each other (Figure 1(c)). With the Petri dish lid on, the biosensors were kept at the PS apex and calibration control point for 30 minutes. The biosensors were then stored in a closed container with a capacity of 2.2 liters for 24 to 48 hours after removing the Petri dish lid. After storage, the gas concentration was measured using a gas detector tube, ethyl acetate detector tube (141L: Gastec, Japan) and a gas sampling pump (GV-100: Gastec).

## 2.2. Laboratory Layout

Figure 2 shows the layout of the laboratory. The laboratory is located on the 4th floor of a 5-story building at 140.10369053 degrees east longitude and 35.63985466 degrees north latitude, and the north side of the laboratory is tilted 3 degrees west of true north. The calibration control point (CCP) is an area of 0.4 m × 0.32 m. The distance between the PS and the CCP is 8.0 m. The top of the PS and the top of the CCP are each 1.8 m above the floor. One aspect of the PS is the direction of magnetic north in November 2009. As of May 2021, magnetic north is estimated to be 7.1 degrees west of true north [18]. True north is the direction that points to the north pole, that is, the northern end of the earth's axis of rotation, 90 degrees north latitude. The layout of the laboratory has not been changed from November 2009 to May 2021.

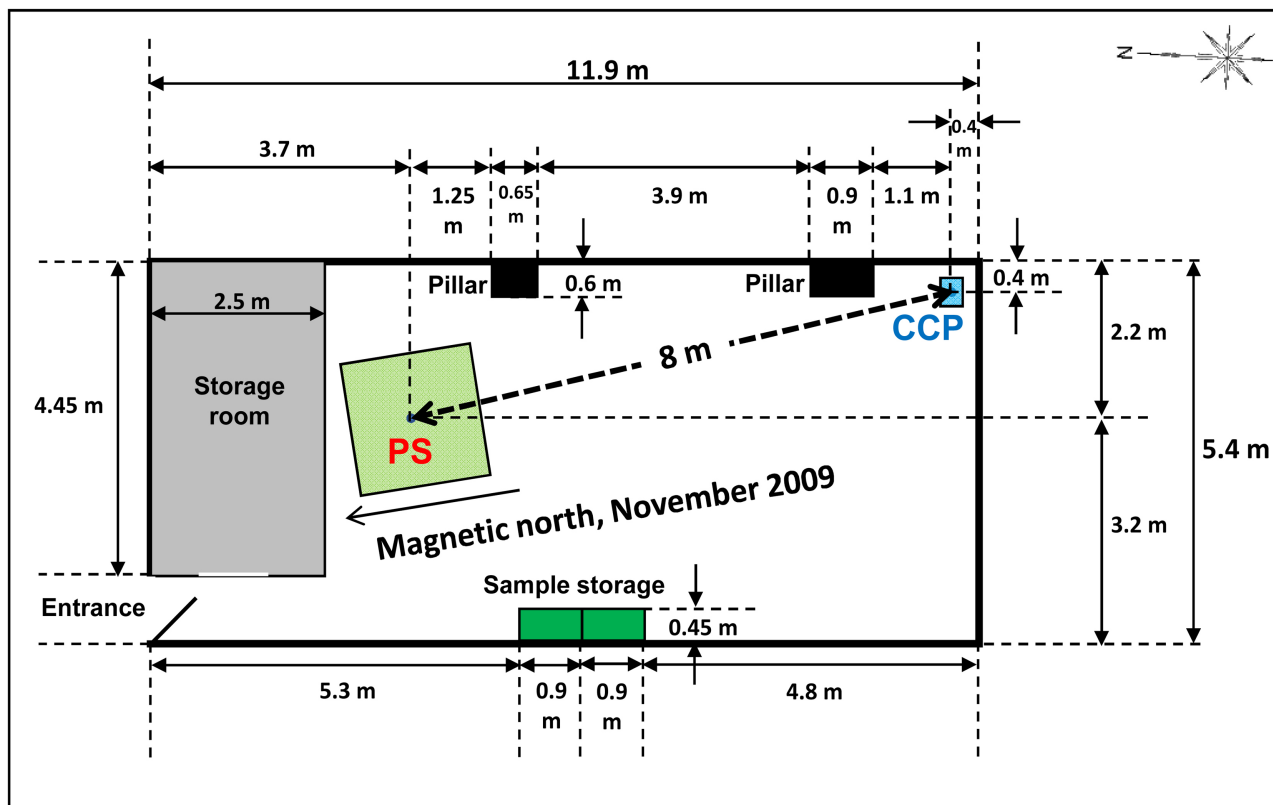


**Figure 2.** Laboratory layout.

### 2.3. Pyramidal Structure

**Figure 3(a)** shows the PS which is a square pyramid with a height of 107 cm, a ridgeline length of 170 cm and a base length of 188 cm. The tilt angle between the bottom and the side of the PS is 49.1°. The base of the PS is raised 73 cm from the floor. The frame of the PS is made of four aluminum pipes, 2 cm in diameter with a 0.36 cm thick pipe wall. Each side has a Sierpinski triangle pattern consisting of 0.3 mm thick aluminum plates. At the top of the PS, a Faraday cage for electrostatic shielding of the biosensors is placed.

**Figure 3(b)** and **Figure 3(c)** show a photograph and a schematic diagram of the PS apex, respectively. When the experimental samples  $G_{E1}$  and  $G_{E2}$  of Pair1 and Pair2 are placed at the PS apex in two layers, the height difference between the two layers is 2 cm. The Petri dish with a large  $G_E$  or  $G_C$  subscript number is on the top, and the Petri dish with a small subscript number is on the bottom. The lower layer is represented as Layer 1 and the upper layer, as Layer 2. The center of the bottom surface of the  $G_{E1}$  Petri dish placed at the PS apex coincides with the point where the center lines of the four aluminum pipes near the PS apex intersect.

## 3. EXPERIMENTAL AND ANALYSIS RESULTS

The data used in the analysis in this paper were the results of experiments conducted between July 2010 and September 2017, excluding the effects of the test subject. The total number of data was  $n = 468$ , which was the same number of as the data analyzed in the previously published papers [7-9].

**Figure 4(a)** shows the average gas concentration of volatile components emitted from the biosensors placed in two layers at the PS apex and the CCP. The plotted results showed the average gas concentrations of the experimental samples,  $(G_{E1} + G_{E2})/2$  and  $(G_{E3} + G_{E4})/2$  were almost the same, as those of the control samples, the results of  $(G_{C1} + G_{C2})/2$  and  $(G_{C3} + G_{C4})/2$ ; in other words, there was no significant

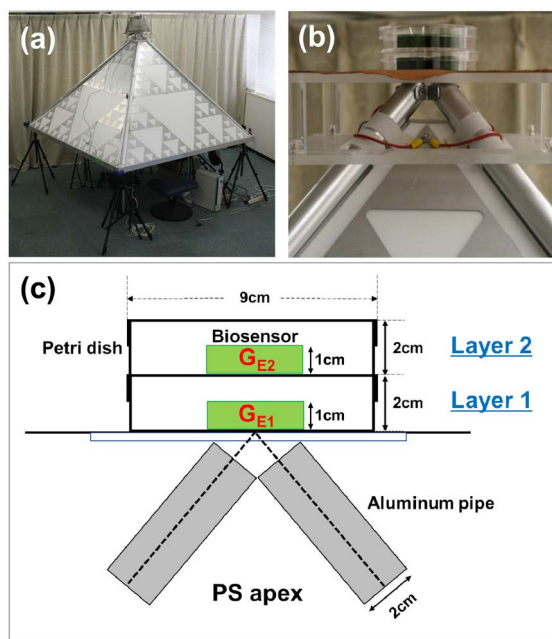


**Figure 3.** (a) Photo of the PS used in the experiment. (b) Photo and (c) schematic drawing of the biosensors placed at the PS apex.

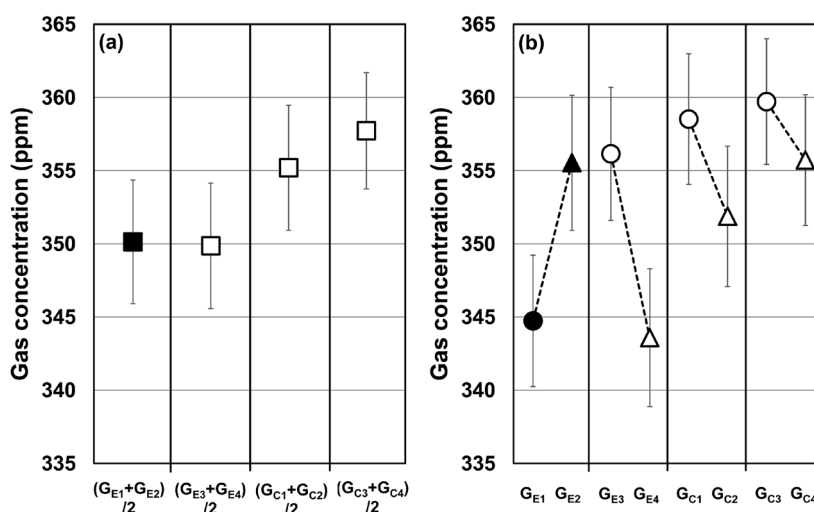


**Figure 4.** Concentration of volatile components released from the biosensors, that is, gas concentration. (a) The average value of the gas concentration in the upper and lower layers of the biosensors placed in two layers. The result for  $(G_{E1} + G_{E2})/2$  placed at the PS apex is represented by the black filled square. The results for  $(G_{E3} + G_{E4})/2$ ,  $(G_{C1} + G_{C2})/2$ ,  $(G_{C3} + G_{C4})/2$  placed at the CCP are represented by open squares. (b) The average value of the gas concentration of each biosensor. The lower layer is represented by circles and the upper layer, by triangles. The results for  $G_{E1}$  and  $G_{E2}$  placed at the PS apex are the black filled symbols, and  $G_{E3}$ ,  $G_{E4}$ ,  $G_{C1}$ ,  $G_{C2}$ ,  $G_{C3}$  and  $G_{C4}$  placed at the CCP are the open symbols. All error bars show the standard error (SE).

difference between the experimental samples and between the control samples. In addition, the control samples tended to have a higher gas concentration than the experimental samples. This characteristic was reported in a previous paper [5], and it was concluded that the gas concentration differed between the experimental samples  $G_E$  and the control samples  $G_C$ , and that this difference was caused by the difference in the directionality of the cut surface. As a result of the analysis, a difference in gas concentration of about 2.2% was detected between the experimental samples  $(G_{E3} + G_{E4})/2$  and the control samples  $(G_{C3} + G_{C4})/2$ . However, as a result of calculating the p-value, a statistically significant difference could not be obtained ( $p = 0.18$ ). The number of data was  $n = 468$ , but we expected that statistical significance would appear as the number of data was increased. **Figure 4(b)** shows the gas concentrations in the lower and upper layers before averaging with respect to the results of the average gas concentration shown in **Figure 4(a)**. In **Figure 4(a)**, the gas concentrations of the experimental samples  $(G_{E1} + G_{E2})/2$  and  $(G_{E3} + G_{E4})/2$  were almost the same. However, in **Figure 4(b)**, the trends of  $G_{E1}$ - $G_{E2}$  and  $G_{E3}$ - $G_{E4}$  showed qualitatively opposite characteristics. That is, the gas concentration of the experimental samples at the PS apex was higher in the upper layer than in the lower layer, and the gas concentration of the experimental samples at the CCP was higher in the lower layer than in the upper layer. In addition, the control samples  $G_{C1}$ - $G_{C4}$  at the CCP tended to have a higher gas concentration in the lower layer than in the upper layer. This characteristic was considered to be the result obtained by the influence of various external environmental conditions (temperature, humidity, atmospheric pressure, etc.) at the CCP. On the other hand, at the PS apex, the gas concentration in the lower and upper layers showed the opposite tendency to the CCP. From this, we inferred that the potential power, “pyramid power”, existed at the PS apex [8].

In this paper, we tried to verify the pyramid effects by analyzing the gas concentration. In this case, there would be no problem in the analysis when handling all data ( $n = 468$ ). However, if all the data were analyzed by dividing them into four seasons, for example, it would be unwise to simply compare and discuss the gas concentration in each season. This is because if the indoor environment differed from season to season, it would be expected that the gas concentration result would differ proportionally. Therefore, in this paper, the analysis was carried out using the values obtained by subtracting the average values of  $G_{C3}$  and  $G_{C4}$  from the gas concentrations of  $G_{E1}$ - $G_{C4}$  shown in **Figure 4(b)**. That is, the control samples  $G_{C3}$  and  $G_{C4}$  placed at the CCP were considered as reference values. The reason why  $G_{C3}$  and  $G_{C4}$  were used as the reference value is explained in detail in the discussion.

**Figure 5** shows the results of calibrating by subtracting the average value of  $G_{C3}$  and  $G_{C4}$  from the results of **Figure 4(b)**. E1 - C4 were calculated by Equation (1).

$$\begin{aligned} E1 &= G_{E1} - (G_{C3} + G_{C4})/2, & E2 &= G_{E2} - (G_{C3} + G_{C4})/2, \\ E3 &= G_{E3} - (G_{C3} + G_{C4})/2, & E4 &= G_{E4} - (G_{C3} + G_{C4})/2, \\ C1 &= G_{C1} - (G_{C3} + G_{C4})/2, & C2 &= G_{C2} - (G_{C3} + G_{C4})/2, \\ C3 &= G_{C3} - (G_{C3} + G_{C4})/2, & C4 &= G_{C4} - (G_{C3} + G_{C4})/2. \end{aligned} \tag{1}$$

Hereinafter, for convenience, E1 and E2 indicate the experimental samples placed at the PS apex, and C1 and C2 are the control samples paired with E1 and E2 placed at the CCP. In addition, E3, E4 and C3, C4 are the paired samples placed at the CCP.

From **Figure 5**, it was seen that the results of E1-C4 were qualitatively the same as those in **Figure 4(b)**. Comparing the control samples C1, C2 and C3, C4 placed at the CCP in two layers indicated the changes were almost the same. On the other hand, when comparing pairs C3, E3 and C4, E4, the values of C4 and E4 in the upper layer were different. This indicated that the rate of change in the gas concentration with respect to the sample in the upper layer was larger than that in the lower layer due to the difference in the direction of the cut surface. In addition, as described in **Figure 4**, the experimental samples E1 and E2 at the PS apex and the experimental samples E3 and E4 at the CCP showed qualitatively opposite changes in the comparison between the lower and upper layers.

The data ( $n = 468$ ) in **Figure 5** were analyzed by dividing them into four seasons, as shown in **Table 1**. The actual start and end days vary from year to year, but in this paper, we set the winter solstice as

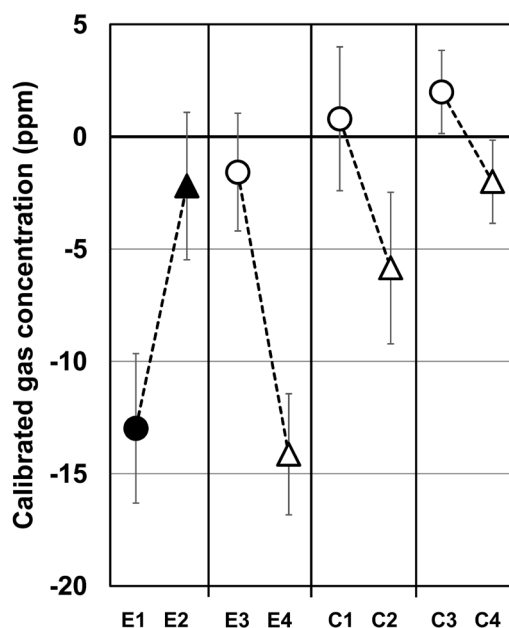


**Figure 5.** Gas concentration calibrated with the average gas concentration of control samples  $G_{C3}$  and  $G_{C4}$  placed at the CCP. Circles are results of the lower layer, triangles are results of the upper layer, the black filled symbols are for the PS apex, and the open symbols are for the CCP. All error bars show the standard error (SE).

**Table 1.** Dividing the data into four seasons.

Classification	Season	Period
WTR	winter	From the winter solstice to the day before the spring equinox 12/22-3/20
SPR	spring	From the spring equinox to the day before the summer solstice 3/21-6/20
SMR	summer	From the summer solstice to the day before the autumn equinox 6/21-9/22
AUT	autumn	From the autumn equinox to the day before the winter solstice 9/23-12/21

12/22, the spring equinox as 3/21, the summer solstice as 6/21, and the autumn equinox as 9/23.

**Figure 6** plots data in four seasons according to the classification in **Table 1**. **Figures 6(a)-(d)**, respectively show WTR ( $n = 84$ ), SPR ( $n = 108$ ), SMR ( $n = 144$ ), and AUT ( $n = 152$ ) results. From them, even if the data were divided into four seasons, they were qualitatively consistent with **Figure 5**, which showed the results for all the data. To summarize, the experimental samples E1 and E2 placed at the PS apex have a higher gas concentration in the upper layer than in the lower layer, and all the samples placed at the CCP have a higher gas concentration in the lower layer than in the upper layer.

**Figure 7** shows the result of overlapping the data of **Figures 6(a)-(d)**. The seasonal deviations of the gas concentrations of C1 and C2 were larger than those of E1-E4 and C3, C4. Among E1-C4, statistically significant differences were detected in the following three cases: 1) WTR and SMR in C1,  $p = 3.3 \times 10^{-3}$ ; 2) WTR and SMR in C2,  $p = 6.0 \times 10^{-4}$ ; and 3) WTR and SPR in C2,  $p = 3.8 \times 10^{-3}$ . Like C3 and C4, C1 and C2 were control samples placed at the CCP, and it was reasonable to think that C1, C2 and C3, C4 were almost equal. However, the results showed that the values were significantly different between C1, C2 and C3, C4. The changes in C3 and C4 and their pair E3 and E4 were almost the same. Therefore, we thought that the abnormal changes in C1 and C2 were caused by the fact that C1 and C2 were paired samples of the experimental samples E1 and E2 at the PS apex. We concluded that the E1 and E2 placed at the

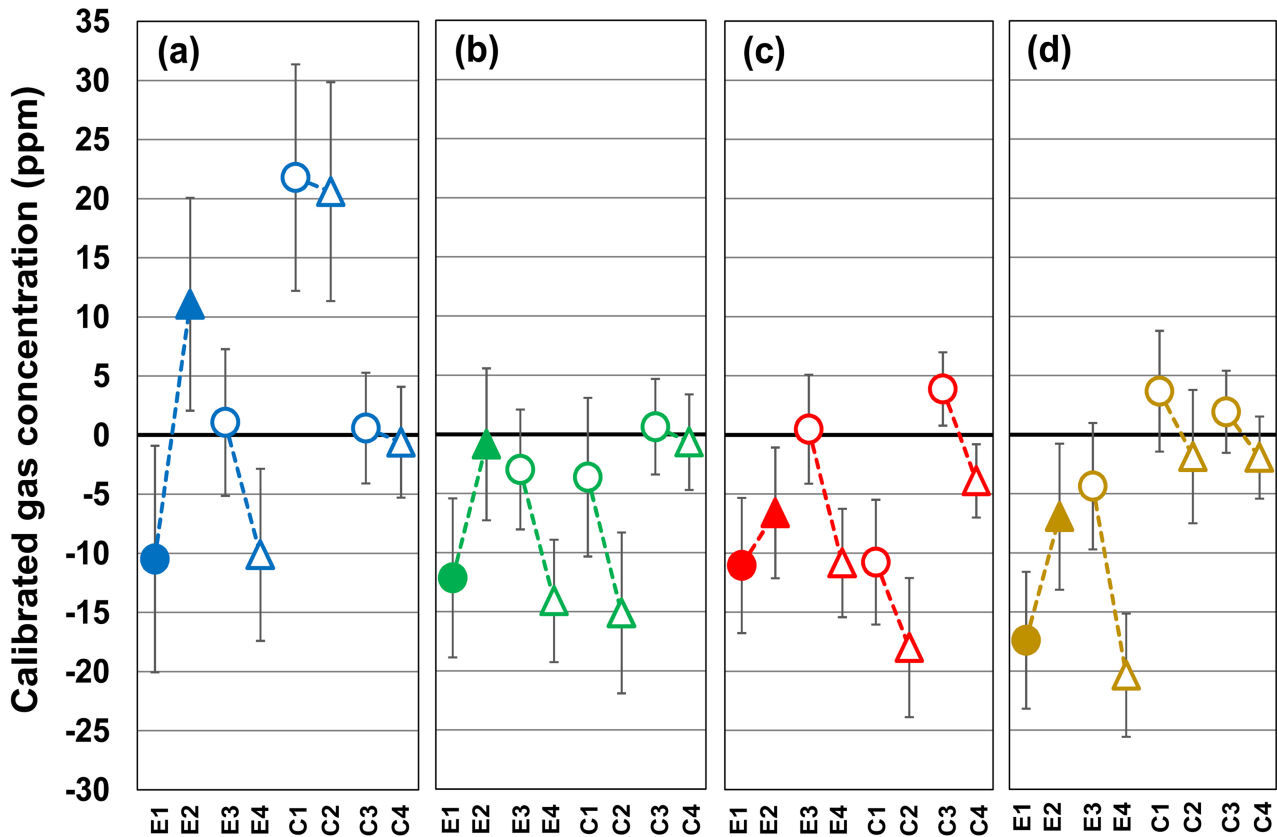


**Figure 6.** Gas concentration calibrated with the average gas concentration of control samples  $G_{C3}$  and  $G_{C4}$  placed at the CCP. (a) WTR (b) SPR (c) SMR (d) AUT. The lower layer biosensors are represented by circles, and the upper layer biosensors, by triangles. The colored filled symbols are results for experimental samples E1, E2 at the PS apex, and the colored open symbols are results for samples E3, E4, C1, C2, C3 and C4 placed at the CCP. All error bars show the standard error (SE).

PS apex were affected by the potential power of the PS, and as a result, some effect was exerted on C1 and C2, which were the paired controls of E1 and E2. From this, we predicted the existence of entanglement between paired samples with the same cut surface. It was clear that the effect on C1 and C2 was not due to the potential power of the PS because if the influence of potential power of the PS extended to the CCP, C3 and C4 should show the same changes as C1 and C2. Furthermore, since significant differences were detected between WTR and SMR in C1 and C2, we expected that the effects of entanglement would vary seasonally.

**Figure 8** shows the seasonal changes in calibrated gas concentration. **Figure 8(a)** and **Figure 8(b)** show the experimental samples E1 and E3 placed in the lower layer and the experimental samples E2 and E4 placed in the upper layer, respectively. **Figure 8(c)** and **Figure 8(d)** show the control samples C1 and C3 placed in the lower layer and the control samples C2 and C4 placed in the upper layer, respectively. **Figure 8(a)** and **Figure 8(b)** show the seasonal changes in the experimental samples E1-E4, and the solid line of E1 and the dotted lines E3 and E4 had qualitatively similar seasonal changes. On the other hand, only the solid line E2 had different seasonal changes. In other words, E2 in the upper layer placed at the PS apex had an abnormal seasonal change. Comparing **Figure 8(a)** and **Figure 8(b)**, the vertical relationship between the solid and the dotted lines was reversed. From this, we predicted that the potential power around the PS apex was present throughout the year. This was consistent with the conclusion pointed out in the previous paper [9] that there was a pyramid effect that did not fluctuate seasonally at the PS apex.

Therefore, we found that the analysis of the gas concentration alone would lead to conclusions about the characteristics of the pyramid effects without introducing the calibrated psi index. A further characteristic was the seasonal variation of the control samples C1-C4 in Figure 8(c) and Figure 8(d). The seasonal changes differed greatly between the solid lines C1 and C2 and the dotted lines C3 and C4. Since the calibration was performed by subtracting the average of the gas concentrations  $G_{C3}$  and  $G_{C4}$ , it could be seen that the seasonal changes of the dotted lines C3 and C4 changed symmetrically around the zero value of the calibrated gas concentration. On the other hand, the solid lines C1 and C2 both had the maximum value with a positive value in WTR and the minimum value with a negative value in SMR. As already shown, a significant difference was detected between WTR value and SMT value in C1 and C2. From this result, it was seen that C1 and C2 had abnormal seasonal changes compared to C3 and C4. And we judged that the abnormality of C1 and C2 was caused by the fact that C1 and C2 were pair samples of E1 and E2 placed at the PS apex, and they were being influenced by E1 and E2. This suggested the existence of entanglement between the cut cucumber sections.

#### 4. DISCUSSION

In this paper, we attempted to verify the pyramid effects only by analyzing the gas concentration emitted from the biosensors, without using the psi index introduced. Here, we describe the psi index in detail. The psi index is calculated by multiplying the natural logarithm of the gas concentration ratio of the paired sample by 100. The relationship between the J value we used before the introduction of the psi index and the psi index  $\Psi$  is  $\Psi = 100J$  [19].

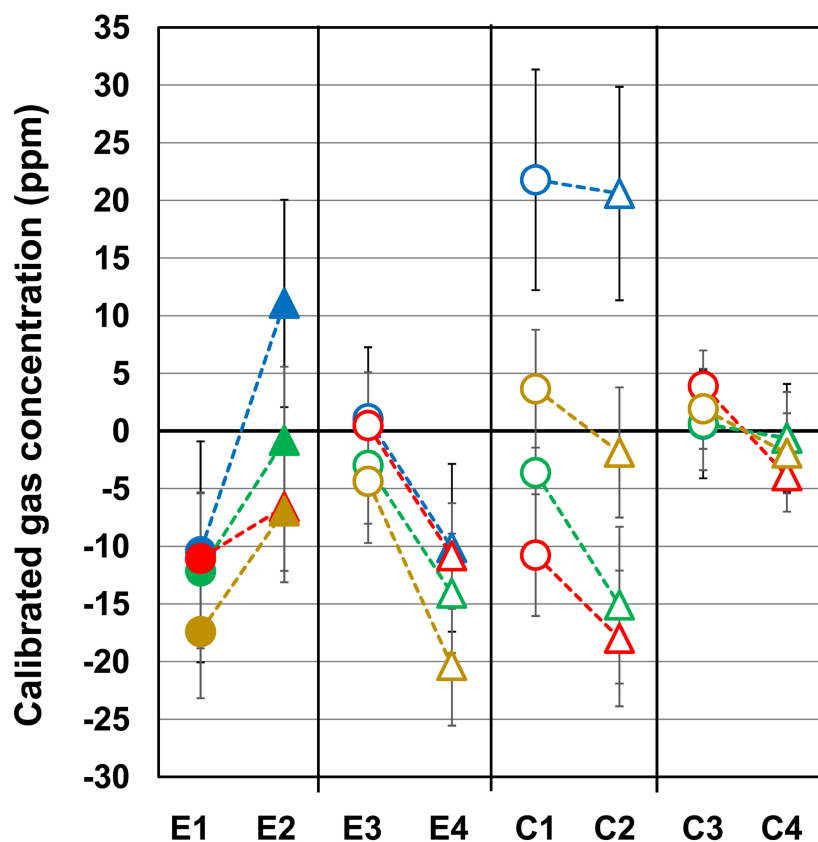


**Figure 7.** Figures 6(a)-(d) are superimposed for display in the graph. Symbols are as explained in the Figure 6 caption. All error bars show the standard error (SE).

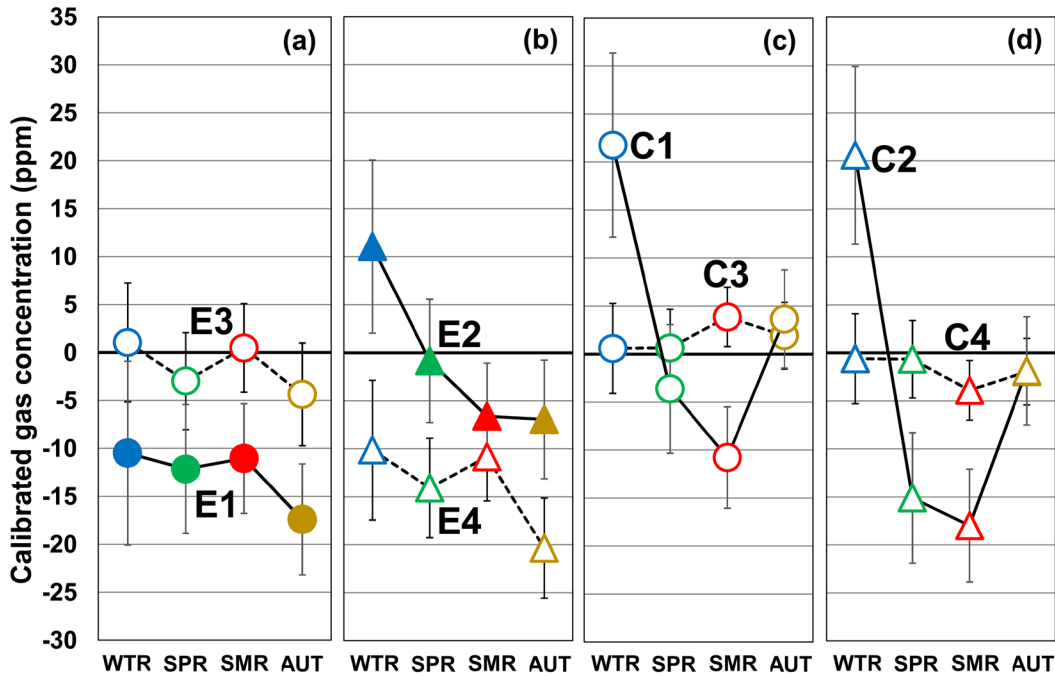


**Figure 8.** Seasonal changes in calibrated gas concentration. (a) Changes in the lower experimental samples: solid line, E1; dotted line, E3. (b) Changes in the upper experimental samples: solid line, E2; dotted line, E4. (c) Changes in the lower control samples: solid line, C1; dotted line, C3. (d) Changes in the upper control samples: solid line, C2, dotted line, C4. Circles represent the lower layer and triangles represent the upper layer. Colored filled symbols represent the biosensors placed at the PS apex, and the colored open symbols represent the biosensors placed at the CCP. All error bars show the standard error (SE).

$$\begin{aligned}
 \Psi_1 &= 100 \ln(G_{E1}/G_{C1}), \\
 \Psi_2 &= 100 \ln(G_{E2}/G_{C2}), \\
 \Psi_3 &= 100 \ln(G_{E3}/G_{C3}), \\
 \Psi_4 &= 100 \ln(G_{E4}/G_{C4}).
 \end{aligned}
 \tag{2}$$

In Equation (2),  $G_{E1}$ - $G_{C4}$  are the measured gas concentrations (ppm).  $\Psi_1$ - $\Psi_4$  are the psi indexes before calibration. In Equation (3),  $\Psi_{1(E-CAL)}$  and  $\Psi_{2(E-CAL)}$  are the calibrated psi indexes of the biosensors placed at the PS apex. These calibrated psi indexes are the results of calibrating the influence of various external environmental conditions such as temperature, humidity, atmospheric pressure and geomagnetism, and the difference in the direction of the cut surface, by the psi index of the CCP. Therefore, the absolute values of  $\Psi_{1(E-CAL)}$  and  $\Psi_{2(E-CAL)}$  represent the magnitude of the pyramid effects.

$$\begin{aligned}
 \Psi_{1(E-CAL)} &= \Psi_1 - (\Psi_3 + \Psi_4)/2, \\
 \Psi_{2(E-CAL)} &= \Psi_2 - (\Psi_3 + \Psi_4)/2, \\
 \Psi_{3(C-CAL)} &= \Psi_3 - (\Psi_3 + \Psi_4)/2, \\
 \Psi_{4(C-CAL)} &= \Psi_4 - (\Psi_3 + \Psi_4)/2.
 \end{aligned}
 \tag{3}$$

The average of the pyramid effects of the PS apex is calculated by Equation (4).

$$\Psi_{(E-CAL)} = (\Psi_{1(E-CAL)} + \Psi_{2(E-CAL)}) / 2. \quad (4)$$

When determining the pyramid effects for the lower and upper layers of the biosensors placed in the two layers at the PS apex, it is necessary to calibrate the difference between the upper and lower when the two layers are stacked. Therefore, the pyramid effects on the lower (Layer1) and upper (Layer2) biosensors are calculated by Equation (5).

$$\begin{aligned} \Psi_{1(E-CAL)Layer1} &= \Psi_{1(E-CAL)} - \Psi_{3(C-CAL)} = \Psi_1 - \Psi_3, \\ \Psi_{2(E-CAL)Layer2} &= \Psi_{2(E-CAL)} - \Psi_{4(C-CAL)} = \Psi_2 - \Psi_4. \end{aligned} \quad (5)$$

$\Psi_{(E-CAL)LayerAve}$  which is the average value of  $\Psi_{1(E-CAL)Layer1}$  and  $\Psi_{2(E-CAL)Layer2}$ , matches  $\Psi_{(E-CAL)}$ .

$$\begin{aligned} \Psi_{(E-CAL)LayerAve} &= (\Psi_{1(E-CAL)Layer1} + \Psi_{2(E-CAL)Layer2}) / 2 \\ &= (\Psi_{1(E-CAL)} + \Psi_{2(E-CAL)}) / 2 = \Psi_{(E-CAL)} \end{aligned} \quad (6)$$

As can be seen from Equation (2), the psi index is obtained by dividing the gas concentration  $G_E$  of the experimental samples by the gas concentration  $G_C$  of the control samples. This is based on the premise that the control samples placed at the CCP can always be a reference and they do not change abnormally. Therefore, it was not possible to predict the possibility of entanglement between the experimental samples and the control samples, which was found by this paper. However, caution is required in the analysis based only on the gas concentration. It is appropriate when dealing with all data, but when analyzing data by dividing it into four seasons, for example, it is not possible to simply compare and examine the average value of the data for each of the four seasons. This is because the external environment of the entire laboratory may differ from season to season, and the effects may be reflected in the gas concentration. However, the same environment is maintained at the PS apex and the CCP for each experiment. As a result, we calibrated and analyzed other gas concentrations based on the average values of  $G_{C3}$  and  $G_{C4}$  at the CCP. Here, the question arises as to why  $G_{C3}$  and  $G_{C4}$  were used as reference values and why  $G_{C1}$  and  $G_{C2}$  should not be used as reference values. Certainly, there should be no problem no matter where the reference value is set, so this is a natural question. We can explain why using **Figure 9**. This figure shows results of calculating E1-C4 using the data of WTR ( $n = 84$ ). Here, **Figure 9(a)** was calculated with  $(G_{E1} + G_{E2})/2$  as the reference value to calculate E1-C4. Similarly, **Figure 9(b)** uses  $(G_{E3} + G_{E4})/2$  as the reference value, **Figure 9(c)** uses  $(G_{C1} + G_{C2})/2$  and **Figure 9(d)** uses  $(G_{C3} + G_{C4})/2$ . **Figures 9(a)-(d)** showed similar changes qualitatively, but **Figure 9(c)** had a shift to the negative side as a whole compared to the others. From this, we decided that it was not appropriate to adopt  $(G_{C1} + G_{C2})/2$  when selecting the reference value. Originally, in the absence of the pyramid effects, the changes in E1-C4 should be qualitatively and quantitatively consistent. This has been confirmed by experiments in which all biosensors of  $G_{E1}$ - $G_{C4}$  were set as CCPs, and no extreme difference appeared in E1-C4.

In an experiment conducted with the expectation that an effect would appear on the experimental samples, two cases were reported in which, contrary to expectations, the effect appeared not on the experimental samples but on the control samples. In the first case, the experiment was done to verify the possibility of affecting the crystallization process of water by the consciousness of many humans, and abnormal results appeared in the control samples instead of the experimental samples [20]. In the second case the experiment was done to verify that the healer affected the emitted gas concentration by focusing on the cucumber biosensor. Despite the fact that the healer was focusing on the experimental samples, the effect appeared on the control samples rather than on the experimental samples [21]. Results for both these cases are considered to be a phenomenon of entanglement related to human consciousness. However, our result is the entanglement that emerges from the potential power of the PS, a non-living object. From this, the potential power of the PS may be “power” similar to human consciousness. It is currently unclear whether the strange phenomenon of entanglement that appears between biosensors due to the potential power of the PS can be understood in relation to quantum entanglement. However, we believe that the possibility cannot be denied.

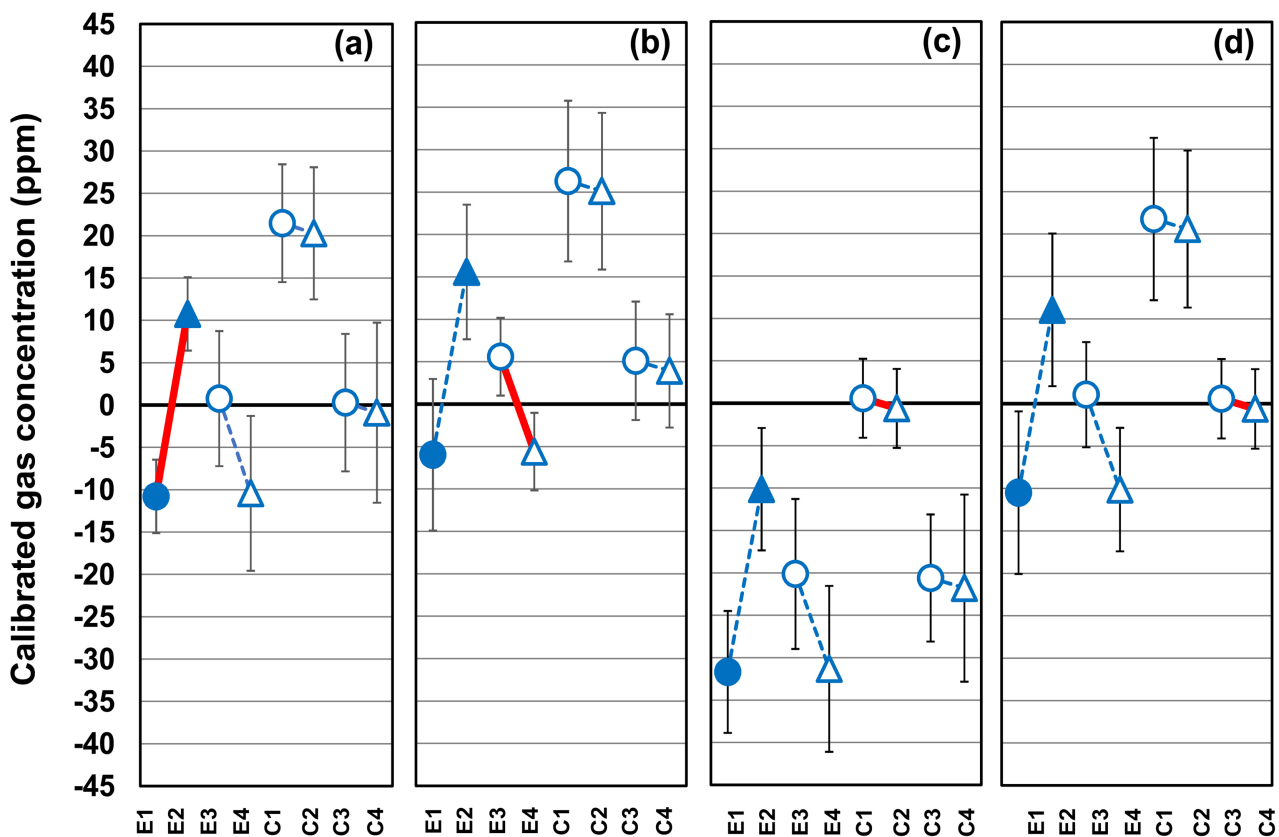


**Figure 9.** E1-C4 results for WTR data. The results of calibration with the reference values of: (a)  $(G_{E1} + G_{E2})/2$ , (b)  $(G_{E3} + G_{E4})/2$ , (c)  $(G_{C1} + G_{C2})/2$ , and (d)  $(G_{C3} + G_{C4})/2$ . The data used as the reference value are shown by the solid red lines. Circles represent the lower layer and the triangles, the upper layer. The filled symbols are the biosensors placed at the PS apex, and the open symbols are the biosensors placed at the CCP.

## 5. CONCLUSIONS

We have introduced the psi index to demonstrate the existence of pyramid effects and to quantitatively treat their magnitude. However, in this paper, when analyzing the pyramid effects due to the potential power of the PS, the analysis was performed using the gas concentration itself without using the psi index. As a result, we were able to discover a phenomenon that has been overlooked so far. It is the phenomenon considered to be entanglement between biosensors created in pairs. In other words, the potential power of the PS affected the experimental samples at the PS apex, which in turn affected the control samples at the calibration control point. It was also clarified that the magnitude of the entanglement effect changed depending on the season. These results gave us new insights into the psi index we introduced. That is, the psi index included not only the pyramid effects on the experimental samples placed at the PS apex, but also the influence of entanglement on the control samples placed at the calibration control point.

Prior to our research, there were few reliable academic studies or statistically significant data on the so-called “pyramid power”. Since 2007, we have been conducting rigorous scientific experiments and analyses using biosensors to elucidate the unexplained “power” of the PS. As a result, we demonstrated the existence of “pyramid power”, which was often perceived as having no scientific basis. While research on “pyramid power” is still often regarded as heretical in the world of academia, our experimental results are the world’s first research results in this field. In the future, we expect that this result will be widely recognized, and will become the basis for a new research field in science, with a wide range of applications.

## CONFLICTS OF INTEREST

The authors declare no conflicts of interest regarding the publication of this paper.

## REFERENCES

1. Takagi, O., Sakamoto, M., Kokubo, H., Yoichi, H., Kawano, K. and Yamamoto, M. (2013) Mediator's Non-Contact Effect on Cucumbers. *International Journal of Physical Sciences*, **8**, 647-651. <https://doi.org/10.5897/IJPS2012.3800>
2. Takagi, O., Sakamoto, M., Yoichi, H., Kokubo, H., Kawano, K. and Yamamoto, M. (2015) Discovery of an Anomalous Non-Contact Effect with a Pyramidal Structure. *International Journal of Sciences*, **4**, 42-51. <https://doi.org/10.18483/ijSci.714>
3. Takagi, O., Sakamoto, M., Yoichi, H., Kokubo, H., Kawano, K. and Yamamoto, M. (2016) An Unknown Force Awakened by a Pyramidal Structure. *International Journal of Sciences*, **5**, 45-56. <https://doi.org/10.18483/ijSci.1038>
4. Takagi, O., Sakamoto, M., Yoichi, H., Kokubo, H., Kawano, K. and Yamamoto, M. (2018) Discovery of Seasonal Dependence of Bio-Reaction Rhythm with Cucumbers. *International Journal of Science and Research Methodology*, **9**, 163-175. <https://www.researchgate.net/publication/331917254>
5. Takagi, O., Sakamoto, M., Yoichi, H., Kokubo, H., Kawano, K. and Yamamoto, M. (2018) Relationship between Gas Concentration Emitted from Cut Cucumber Cross Sections and Growth Axis. *International Journal of Science and Research Methodology*, **9**, 153-167. <https://www.researchgate.net/publication/331917255>
6. Takagi, O., Sakamoto, M., Yoichi, H., Kokubo, H., Kawano, K. and Yamamoto, M. (2019) Discovery of an Unexplained Long-Distance Effect Caused by the Association between a Pyramidal Structure and Human Unconsciousness. *Journal of International Society of Life Information Science*, **37**, 4-16. [https://doi.org/10.18936/islis.37.1\\_4](https://doi.org/10.18936/islis.37.1_4)
7. Takagi, O., Sakamoto, M., Yoichi, H., Kawano, K. and Yamamoto, M. (2019) Potential Power of the Pyramidal Structure. *Natural Science*, **11**, 257-266. <https://doi.org/10.4236/ns.2019.118026>
8. Takagi, O., Sakamoto, M., Yoichi, H., Kawano, K. and Yamamoto, M. (2020) Potential Power of the Pyramidal Structure II. *Natural Science*, **12**, 248-272. <https://doi.org/10.4236/ns.2020.125022>
9. Takagi, O., Sakamoto, M., Yoichi, H., Kawano, K. and Yamamoto, M. (2020) Potential Power of the Pyramidal Structure III: Discovery of Pyramid Effects with and without Seasonal Variation. *Natural Science*, **12**, 743-753. <https://doi.org/10.4236/ns.2020.1212066>
10. Kokubo, H. and Yamamoto, M. (2009) Controlled Healing Power and Ways of Non-Contact Healing. *Journal of International Society of Life Information Science*, **27**, 90-105. [https://doi.org/10.18936/islis.27.1\\_90](https://doi.org/10.18936/islis.27.1_90)
11. Kokubo, H., Takagi, O., Koyama, S. and Yamamoto, M. (2011) Discussion of an Approximated Equation for Special Distribution of Controlled Healing Power around a Human Body. *Journal of International Society of Life Information Science*, **29**, 23-34. [https://doi.org/10.18936/islis.29.1\\_23](https://doi.org/10.18936/islis.29.1_23)
12. Kokubo, H. (2015) Ki or Psi—Anomalous Remote Effects of Mind-Body System. Nova Science Publishers, Inc., New York.
13. Farmer, E.E. (2013) Surface-to-Air Signals. *Nature*, **411**, 854-856. <https://doi.org/10.1038/35081189>
14. Ozawa, R., Arimura, G., Takabayashi, J., Shimoda, T. and Nishioka, T. (2000) Involvement of Jasmonate- and Salicylate-Related Signaling Pathways for the Production of Specific Herbivore-Induced Volatiles in Plants. *Plant and Cell Physiology*, **41**, 391-398. <https://doi.org/10.1093/pcp/41.4.391>
15. De Moraes, C.M., Lewis, W.J., Paré, P.W., Alborn, H. T. and Tumlinson, J.H. (1998) Herbivore-Infested Plants Selectively Attract Parasitoids. *Nature*, **393**, 570-573. <https://doi.org/10.1038/31219>
16. De Moraes, C.M., Mescher, M.C. and Tumlinson, J.H. (2001) Caterpillar-Induced Nocturnal Plant Volatiles Repel Conspecific Females. *Nature*, **410**, 577-580. <https://doi.org/10.1038/35069058>
17. Goodspeed, D., Liu, J.D., Chehab, E.W., Zheng, Z., Francisco, M., Kliebenstein, D.J. and Braam, J. (2013) Postharvest Circadian Entrainment Enhances Crop Pest Resistance and Phytochemical Cycling. *Current Biology*, **23**, 1235-1241. <https://doi.org/10.1016/j.cub.2013.05.034>

18. Geospatial Information Authority of Japan. [https://www.gsi.go.jp/buturisokuchi/menu01\\_index.html](https://www.gsi.go.jp/buturisokuchi/menu01_index.html)
19. Kokubo, H., Takagi, O. and Yamamoto, M. (2009) Development of a Gas Measurement Method with Cucumbers as a Bio-Sensor. *Journal of International Society of Life Information Science*, **27**, 200-213. [https://doi.org/10.18936/islis.27.2\\_200](https://doi.org/10.18936/islis.27.2_200)
20. Radin, D., Lund, N., Emoto, M. and Kizu, T. (2008) Effects of Distant Intention on Water Crystal Formation: A Triple-Blind Replication. *Journal of Scientific Exploration*, **22**, 481-493. <https://www.researchgate.net/publication/255669110>
21. Kokubo, H., Takagi, O. and Koyama, S. (2011) Application of a Gas Measurement Method: Measurement of Ki-Fields and Non-Contact Healing. *Journal of International Society of Life Information Science*, **28**, 95-103. [https://doi.org/10.18936/islis.28.1\\_95](https://doi.org/10.18936/islis.28.1_95)